

DTI Longitudinal Atlas Construction as an Average of Growth Models

Gabriel Hart¹, Yundi Shi¹, Hongtu Zhu¹,
Mar Sanchez², Martin Styner¹, and Marc Niethammer¹

UNC Chapel Hill¹ and Emory University²

Abstract. Existing atlas-building methods for diffusion-tensor images are not designed for longitudinal data. This paper proposes a novel longitudinal atlas-building framework explicitly accounting for temporal dependencies of longitudinal MRI data. Subject-specific growth modeling, cross-sectional atlas-building and growth modeling in atlas space are combined with statistical longitudinal modeling, resulting in a longitudinal diffusion tensor atlas. The method captures changes in morphology, while modeling temporal changes and allowing to account for covariates. The component algorithms are based on large-displacement metric mapping formulations. To effectively account for measurements sparse in time, a continuous-discrete growth model is proposed. The method is applied to a longitudinal dataset of diffusion-tensor magnetic resonance brain images of developing macaque monkeys with time-points at ages 2 weeks, 3 months, and 6 months.

1 Introduction

The study of time-dependent image data is of fundamental importance in medical image analysis. The ability to observe change over time in a population of subjects can yield insight into the function and development of biological systems. Longitudinal studies that aim to observe such changes acquire images from each subject in a population at multiple points in time, thus capturing subject-specific development trajectories. Only few time-points are typically available.

Magnetic resonance imaging (MRI) has revolutionized neuroscience. Structural MR imaging is in routine clinical use and special MR scanning sequences to for example probe water diffusion or blood oxygenation levels have become indispensable tools for neuroscience. Atlas-based methods are used extensively for the analysis of MR data, in particular, to provide a common coordinate frame for the analysis of subject populations. But even though the importance of age-specific atlases has been established [19], longitudinal information has only been used to a limited extent in atlas-building. This is undesirable since longitudinal atlases promise a better characterization of neurodevelopment which is not fully understood. For example, while there are neuroanatomical descriptions of early brain maturation in the monkey [14], information on the normal postnatal maturation of the monkey brain especially during the peripubertal phase remains limited. To characterize brain development, a longitudinal brain atlas would be

highly useful. Combined with statistical information, a normative atlas could also be used to characterize deviations from the norm for pathologies.

The goal of this paper is to propose a novel longitudinal atlas-building framework explicitly accounting for temporal dependencies of longitudinal MRI data. In particular, a continuous-discrete (continuous time dynamics and discrete time measurement) formulation is proposed to address the sparse measurements in time. The new method is applied to construct a longitudinal diffusion-tensor (DT) atlas from DT datasets for seven macaque monkeys ranging from two weeks in age to six months, each with three measured time-points. Since the method is general, it could conceivably be used on similar data, for example for data from the NIH MRI study of normal brain development [7].

Sec. 2 discusses the works of Davis et al. [5] and Durrleman et al. [6] and how they relate to the proposed method. Sec. 3 details the setup and procedure for the longitudinal atlas construction algorithm. Results are presented in Sec. 4. The paper concludes with an outlook on future work.

2 Background

There are few approaches for atlas-building which can be used for *longitudinal data*. Existing approaches are: (1) atlas-building by registration of cross-sectional atlases, (2) atlas-building by concatenation of 3D atlases followed by 4D registration [16], (3) atlas-building by regression [5], and (4) atlas-building by joint alignment of image time-series [6]. Only the recent work by Durrleman et al. [6] utilizes subject-specific longitudinal information. Other existing atlas-building schemes typically treat measurements as independent and perform a variant of cross-sectional atlas-building. The method proposed in this paper uses longitudinal information and is most closely related to [5,6].

Davis et al. [5] use a weighting kernel over time to compute an average image at a given atlas time-point as the point in space that minimizes the time-weighted squared distance to all measured images. The method allows for images measured at arbitrary points in time. While it can be applied to longitudinal data, subject-specific temporal relationships are disregarded; all measurements are treated independently. See Fig. 2 (a) for an illustration of the method.

Durrleman et al. [6] formulate longitudinal atlas-building as a single optimization problem incorporating subject-specific growth models matched to an estimated longitudinal atlas; potential time-shifts are also accounted for. To measure compliance of an individual’s growth curve with respect to a current atlas-estimate, the growth trajectory is brought into atlas-space by applying an identical (estimated) diffeomorphic map for all its time-points. The registration method is based on currents and the method is applied to surfaces in two- and three spatial dimensions. Fig. 2 (b) illustrates the overall process.

This paper discusses a conceptually simple approach to build longitudinal atlases using diffusion tensor images. In contrast to previous work, the proposed method: (1) uses a four-step atlas-building strategy, which combines individual growth modeling with cross-sectional atlas-building at time-point-adjusted image volumes and growth-modeling in atlas-space, (2) performs longitudinal

atlas-building for diffusion tensor images, and (3) is combined with a statistical modeling step working directly with diffusion tensors, which can take full advantage of the longitudinal data and in particular allows for the computation of estimation statistics (such as covariances over the population), can account for covariates, and facilitates hypothesis testing (though the latter point is not explored in this paper).

Since the study of neurodevelopment is the primary driving biological problem for the development of the proposed approach, focusing initially on diffusion tensor atlases is beneficial with fiber structure already discernible at a very early stage of neurodevelopment. This greatly simplifies the registration of image time-series in comparison to structural images, which experience contrast inversion – see Fig. 1 for an illustration.

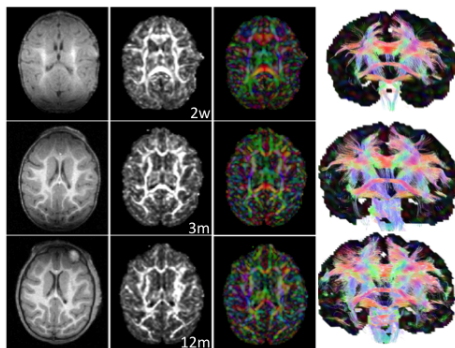


Fig. 1. T1 (left column), FA (middle left column), color by orientation (middle right column) axial slices and 3D tractography results (right) for a 2 week (top row), 3 months (middle row) and 12 months old (bottom row) macaque. Contrast inversion greatly changes the appearance of the structural MR images throughout development. However, diffusion information is more stable across time simplifying registration of image time-series.

3 Methodology

As shown in Fig. 2, the proposed longitudinal atlas-building method makes use of continuous-discrete growth modeling (Sec. 3.1), time-adjusted cross-sectional atlas building (Sec. 3.2), and statistical longitudinal modeling (Sec. 3.3), resulting in a tensor-valued longitudinal atlas. Preprocessing consists of affine alignment of all images based on histogram quantile normalized fractional anisotropy (FA) images, to the histogram of the oldest image in the population. Normalization is useful to compensate for the changes of FA range during brain development (since diffusion anisotropy in the brain increases with age [12]). Note that while full tensor-based registration methods [2,15,18] could be used for all the registration steps, the registrations are performed with a rotationally invariant measure (FA) for simplicity. The pre-processed FA image set is denoted as $\{I^{(i,t)}\}$. Fig. 3 illustrates the overall pipeline described in detail in the following sections.

3.1 Single Subject Growth Modeling

The goal of individual growth modeling for subject s with corresponding image set $\{I^{(s,t)}\}$ is to recover the geometric change occurring between each measured

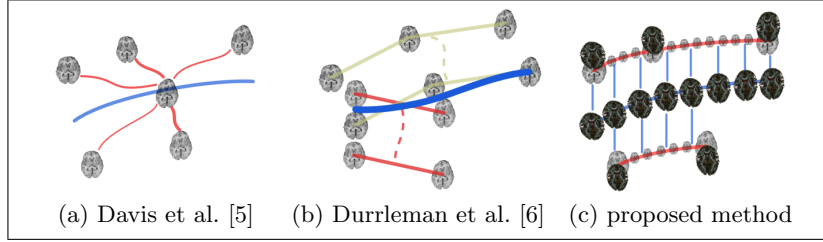


Fig. 2. Atlas construction methods: (a) Each atlas time-point is computed as an average of all images in the population weighted by a kernel on temporal distance. (b) The atlas is computed such that it is the best alignment of a set of image time-series (growth models). Differences are measured in atlas space, where all time-series time-points are transformed by the same diffeomorphism from subject to atlas space. Temporal alignments are also considered. (c) The proposed method builds cross-sectional atlases based on time-adjusted measurement images (as obtained from subject-specific growth models). This establishes spatial correspondences between all subjects and all subject time-points. Statistical longitudinal modeling based on these correspondences is used to estimate the average diffusion tensors over space and time.

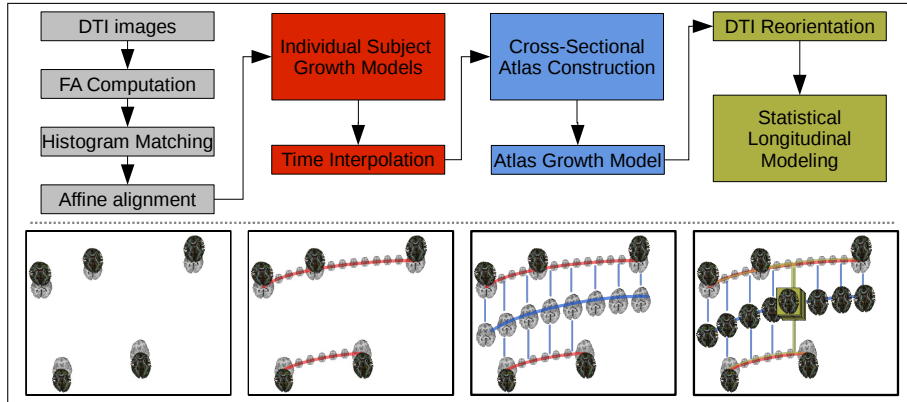


Fig. 3. Longitudinal atlas construction: The pipeline consists of four steps: Image preprocessing, individual subject growth modeling (Sec. 3.1), cross-sectional atlas construction (Sec. 3.2), and statistical longitudinal modeling (Sec. 3.3).

time-point. Since large deformations are possible throughout brain development, a form of fluid registration is sensible. Here, a variant of large displacement diffeomorphic metric mapping (LDDMM) [4,11] adapted to time-series is used following [13]. Measurements are assumed sparse in time, while subject growth is assumed to be time-continuous. The minimizer of

$$E(v, \bar{I}^{(s,t_0)}) = \int_{t_0}^{t_T} \|v\|_V^2 dt + \frac{1}{\sigma^2} \sum_{i=0}^T \|I^s(t_i) - I^{(s,t_i)}\|_{L_2}^2, \quad (1)$$

$$s.t. \quad \frac{\partial I^s}{\partial t} + \nabla I^s \cdot v = 0, \quad I^s(t_0) = \bar{I}^{(s,t_0)}, \quad (2)$$

where $I^s(t)$ is the continuous image estimate for subject s at time t , v is a time-dependent velocity field, and $\bar{I}^{(s,t_0)}$ denotes a template image will result (given an appropriately chosen norm $\|\cdot\|_V$) in a piecewise-diffeomorphic interpolation path approximating the images $\{I^{(s,t_i)}\}$ at their respective measurement times. Here, t_0 denotes the youngest measured time-point for subject s and t_T the oldest and σ is a constant trading off accuracy in image matching (small σ) and smoothness in the deformation field (large σ). This is a dynamically constrained energy minimization problem. (Such a model without template estimation has been used in [6,9]). The optimality conditions are

$$I_t^s + \nabla I^s \cdot v = 0, \quad I^s(t_0) = \bar{I}^{(s,t_0)}, \quad \bar{I}^{(s,t_0)} = \frac{\sum_{i=0}^T |D\Phi_{t_0,t_i}^s| I^{(s,t_i)} \circ \Phi_{t_0,t_i}^s}{\sum_{i=0}^T |D\Phi_{t_0,t_i}^s|}, \quad (3)$$

for the interpolated images. Here, for each measured image $I^{(s,i)}$ and a given time \hat{t} , $\Phi_{\hat{t},t_i}^s$ is the diffeomorphism that maps from the coordinate frame at time \hat{t} to the coordinate frame at time t_i . It is the solution to the transport equation

$$\frac{\partial \Phi^s}{\partial t} + D(\Phi^s)v = 0, \quad \Phi^s(t_i) = id \quad (4)$$

on the interval from t_i to \hat{t} , where D is the Jacobian and id denotes the identity map. For the adjoint variable λ (the Lagrangian multiplier used to enforce the transport equation of Eq. 2 as a dynamic equality constraint)

$$-\lambda_t^s - \text{div}(\lambda^s v) = 0, \quad \begin{cases} \lambda^s(t_T(-)) = \frac{2}{\sigma^2}(I^{(s,t_T)} - I^s(t_T)) \\ \lambda^s(t_i(-)) = \lambda^s(t_i(+)) + \frac{2}{\sigma^2}(I^{(s,t_i)} - I^s(t_i)), \end{cases}$$

needs to hold piecewise ($(-)$ and $(+)$ denote the left- and the right-sided values at a given time-point). The state I , the adjoint λ , and the velocity field v , further need to fulfill the optimality condition

$$\nabla E_v = 2L^\dagger Lv + \nabla I^s \lambda^s = 0,$$

which can be used to compute the energy gradient with respect to v^1 .

Given a $\{v, \bar{I}^{(s,t_0)}\}$, the time-dependent velocity field v can be used to compute an image at any time-point between t_0 and t_T either by directly solving the transport equation 2 or by applying the diffeomorphic map $\Phi_{\hat{t},t_i}^s$ (see [13] for details on the numerical solution method). For the optimal $\{v, \bar{I}^{(s,t_0)}\}^*$ the maps (velocity fields v receptively) can be used to geometrically align all images of the time-series. Note that this formulation allows joint estimation of the velocity field and a template image $\bar{I}^{(s,t_0)}$. This is a useful feature, in particular, if image measurements are staggered in time, since the template estimation avoids fixing an explicit time origin for the growth model (as typically done). For the experimental data in this paper $\bar{I}^{(s,t_0)} := I^{(s,t_0)}$, since all image time-series are measured at the same time-points (2 weeks, 3 months, and 6 months).

¹ v and T are also subject-dependent. This dependency is suppressed for notational clarity.

3.2 Cross-Sectional Atlas Construction

To account for possible appearance changes in the atlas-building for a chosen time-point t , images are interpolated using a voxel-wise average $I^s(\hat{t})$ using the maps obtained in the growth modeling step such that

$$\hat{I}^s(\hat{t}) = \frac{\sum_{i=0}^T w_i (I^{(s,t_i)} \circ \Phi_{\hat{t},t_i}^s)}{\sum_{i=0}^T w_i}. \quad (5)$$

Here, w_i are interpolation weights. For the experiments in this paper linear interpolation is used to provide a simple baseline algorithm, but more sophisticated interpolation methods are conceivable. For example, a time-series adaptation of metamorphosis [17] could be used to simultaneously determine the maps as well as a change in image appearance.

Given the appearance-adjusted images $\{\hat{I}^s(t)\}$ for all subjects, for a time-point t , the cross-sectional atlas is computed as the Fréchet mean of $\{\hat{I}^s(t)\}$ [8], minimizing the sum of squared differences to all images:

$$\tilde{I}(t) = \operatorname{argmin}_{I_T} \sum_{i=1}^n d(\hat{I}^i(t), I_T)^2, \quad \text{where} \quad (6)$$

$$d(\hat{I}^i(t), I_T)^2 = \min_{\hat{\Phi}_{1,0}^{(i,t)}} \int_0^1 \|v^i\|_V^2 dt + \frac{1}{\sigma^2} \|\hat{I}^i(t) \circ \hat{\Phi}_{1,0}^{(i,t)} - I_T\|_{L_2}^2. \quad (7)$$

Here, n is the total number of subjects and $\hat{\Phi}_{1,0}^{(i,t)}$ is the coordinate map from subject i to the atlas space for the given atlas time-point at t . This paper uses a full space-time discretization instead of the standard greedy implementation.

After all cross-sectional atlas time-points $\tilde{I}(t)$ have been computed, the growth modeling technique of Sec. 3.1 is used to recover the inter-atlas growth trajectory. This step results in a complete set of spatial correspondences between all subjects and all time-points.

3.3 Statistical Longitudinal Modeling

Statistical longitudinal models are computed for each growth trajectory using the spatial correspondences of Sec. 3.2. Given a chosen reference time-point \hat{t} all original DTI images are aligned with respect to the atlas space $\tilde{I}(\hat{t})$. The diffeomorphism from any given measured image $I^{(i,t)}$ to the reference atlas image $\tilde{I}(\hat{t})$ are computed by composing the intra-subject map $\Phi_{\hat{t},t}^i$ that transforms $I^{(i,t)}$ to time-point \hat{t} (blue in Fig. 4), with the inter-subject map $\hat{\Phi}_{1,0}^{(i,\hat{t})}$ that transforms $I^i(\hat{t})$ to the atlas space (red in Fig. 4)

$$\Phi_{A(\hat{t}), (i,t)} = \hat{\Phi}_{1,0}^{(i,\hat{t})} \circ \Phi_{\hat{t},t}^i. \quad (8)$$

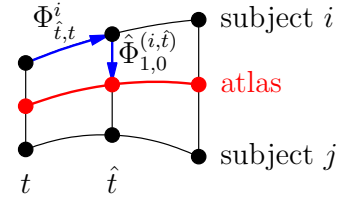


Fig. 4. Transformation from subject space time-point t to atlas at time \hat{t} .

The tensors $\{\mathcal{T}^{(i,t)}\}$ are reoriented according to their respective space transformations following [1]. After spatial normalization, a generalized estimating equation (GEE) is used to explicitly model the longitudinal growth of DTI, while controlling for other covariates of interest, such as gender, denoted by $\mathbf{x}_{ij} = (x_{ij1}, \dots, x_{ijq})^T$ for the i -th subject at the j -th time-point for $i = 1, \dots, n$ and $j = 1, \dots, m_i$. The diffusion tensors $D_{i,j}$ at each voxel are log-transformed [3], denoted by $\log(D_{i,j})$ and a moment model is assumed for $\log(D_{i,j})$, which is given as follows:

$$E(\log(D_{i,j})) = \mu_{ij} = x_{ij1}\beta_1 + \dots + x_{ijq}\beta_q \quad \text{for } j = 1, \dots, m_i, \quad (9)$$

where β_k are the unknown 6×1 vectors. Compared with the standard general linear models, model (9) based on the conditional mean and covariance of ϵ_i avoids assuming the distributional assumption of imaging measures. It is desirable for the analysis of log-transformed diffusion tensors, because the distribution of $\log(D_{i,j})$ may deviate significantly from a multivariate Gaussian distribution.

Because neuroimaging measures $(\log(D_{i,1}), \dots, \log(D_{i,m_i}))^T$ from the same subject are often positive correlated, it is assumed that $\text{Cov}(\mathbf{Y}_i)$ can be decomposed as $A_i^{1/2}(\xi)R_i(\alpha)A_i^{1/2}(\xi)$, where A_i is a diagonal matrix of the variances of $\log(D_{i,j})$, in which ξ is a common parameter vector. In addition, the working correlation matrix $R_i(\alpha)$ represents the correlation among the m_i repeated measurements over time, where α is a vector of parameters. Commonly used working correlation structures include independence structure, exchangeable structure, autoregressive structure, and other structures. Then, by following Liang and Zeger [10], a GEE for β and other parameters in ξ and α is constructed and the unknown parameters are estimated iteratively.

In real applications, it is common to test linear hypotheses of β in order to answer various scientific questions involving a comparison of diffusion tensors across two (or more) diagnostic groups or the changes of diffusion tensors across time. These questions can be formulated as testing linear hypotheses of β as follows: $H_0 : R\beta = \mathbf{b}_0$ vs. $H_1 : R\beta \neq \mathbf{b}_0$, where R is an $r \times p$ matrix of full row rank and \mathbf{b}_0 is an $r \times 1$ specified vector. The null hypothesis $H_0 : R\beta = \mathbf{b}_0$ is tested using a score test statistic or a Wald statistic, denoted by S_n . The statistic S_n is approximately distributed as $\chi^2(r)$, a chi-square distribution with r degrees of freedom. To control the family-wise error rate, the maxima of the score test statistics are considered, defined by $S_{\mu, \mathcal{D}} = \max_{d \in \mathcal{D}} S_n(d)$. To use $S_{\mu, \mathcal{D}}$ as test statistics, a test procedure that is based on the resampling method to approximate the distribution of $S_{\mu, \mathcal{D}}$ is used. This procedure is essentially a wild bootstrap method for the hypothesis test.

4 Results

The proposed longitudinal atlas building method was applied to scans from an ongoing study of neurodevelopmental alterations caused by infant maltreatment in rhesus macaque monkeys. Ten macaques were scanned longitudinally at ages of two weeks (neonate), three months and six months. Following birth, subjects

were cross-fostered in randomized fashion creating 4 groups allowing for the measurement of both exposure to physical abuse (by abusive macaque mothers) as well as genetic predisposition. In addition to the group designations, the following known covariates were used in the longitudinal atlas modeling: weight at birth, gender, and postnatal age (in days) at scan.

Scans were acquired at the Yerkes Imaging Center, Emory University, on a 3T Siemens Trio scanner with 8-channel phase array trans-receiving volume coil. High-resolution T1-weighted and T2-weighted MRI scans were acquired first, followed by the DTI scans (voxel size: 1.3x1.3x1.3mm³ with zero gap, 60 directions, TR/TE=5000/86 ms, 40 slices, FOV: 83 mm, b:0, 1000 s/mm², 12 averages). The whole scanning procedure took 2-3 hours with 75 minutes dedicated to the DTI scan for each monkey kept under monitored anesthesia using isoflurane (1-1.5%) following an initial injection of telazol (4-5 mg/kg).

The longitudinal tensor atlas was computed for seven subjects (3 control females, 2 abused females, and 2 abused males who already had images acquired at the three time-points) using the proposed method of Sec. 3². To illustrate the benefit of computing an average longitudinal atlas over an individual time-series, Fig. 5 shows the result of single subject growth model (corresponding to the first pipeline step). The initial affine alignment registers the overall structures well, removing large-scale size differences due to brain growth, showing that for this particular subject brain morphology does not change drastically during the first six months of neurodevelopment. Signal to noise ratio is relatively low for an individual subject leading to noisy patterns of local expansion and contraction.

Fig. 6 shows the results of the geometric alignment of subjects at different time-points to a reference atlas as needed for the statistical longitudinal modeling step. The figure shows six of the initial FA images aligned to the cross-sectional atlas at the 97 day time-point as well as the computed atlas image. Good alignment is achieved. Structures in the difference images mainly represent changes in FA which could not be compensated through histogram equalization, rather than large-scale inaccuracies in the image alignment.

Fig. 7 shows the results of the full longitudinal atlas construction after the final time-series has been computed over the cross sectional atlases. Resulting atlas images show (as expected) significantly higher signal to noise ratios compared to images from an individual subject. Further, a clearer pattern of local expansion and contraction emerges, showing for example an expansion in the area between the internal capsule and the external capsule.

Finally, Fig. 8 shows the diffusion tensor results calculated using statistical longitudinal modeling correcting for gender, birthweight, and group (control or abused). The results show a distinct increase in diffusion between two weeks and six months (brighter colors in the color by orientation images).

² Note that the this paper aims at showing example results for the proposed method. To construct an atlas of normal brain development usable for population studies, an appropriate subject population should be chosen.

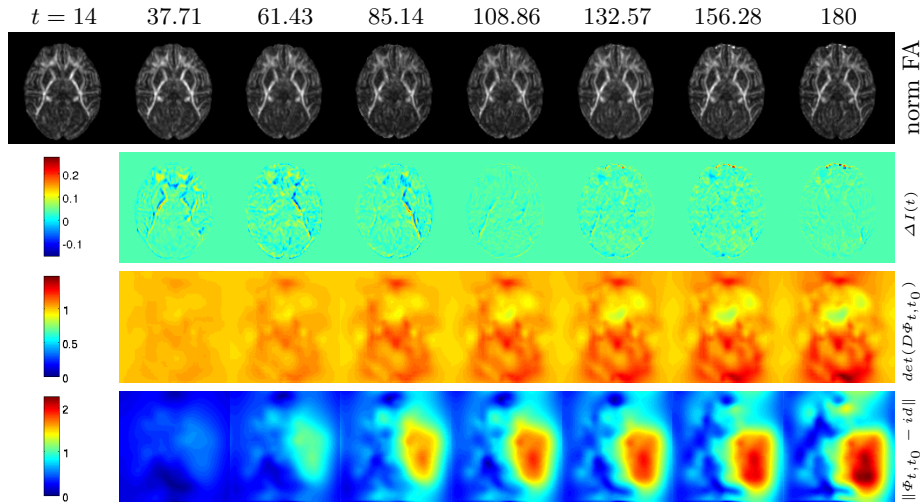


Fig. 5. Growth modeling results. [Top] Central axial slices from the growth model of a male subject show the progression of growth from 2 weeks (14 days) through 6 months (180 days). Images are generated using the interpolation process described in Section 3.1. [Middle, top] Difference images computed between each growth image demonstrate the locations of growth between each time-point. Red indicates raised intensity and blue indicates lowered intensity. [Middle, bottom] The determinant of the Jacobian of the coordinate map illustrates the local expansion and contraction of the evolving model with respect to $t = 14$. Since backward maps (maps from time-point t to $t = 14$) are used, values over 1 indicate local contraction while values under 1 indicate local expansion. [Bottom] The magnitude of displacement with respect to the initial time-point shows deformations (in mm) and indicates some asymmetry for this subject.

5 Conclusion and Future Work

This paper presented a novel approach for longitudinal atlas construction using DT-MRI images. The method was applied to seven subjects from a database of developing rhesus macaque monkeys, each with measured images at two weeks, three months, and six months of age. Modeling the growth of each subject individually before modeling the growth of the entire population, takes advantage of the longitudinal nature of the data set. Statistical longitudinal modeling was used to produce the average tensors over the time span of the data, while accounting for associated covariates, such as gender and birthweight.

Future work will use a much larger number of subjects to compute an atlas of normal brain development for the macaque. Statistical modeling will then also be used to compute measures of atlas variance (which can be handled by the framework, but requires more than the currently available seven subjects in the study) and to perform hypothesis testing for population studies. Longitudinal monkey atlases will be made available as a resource for primate MRI studies and

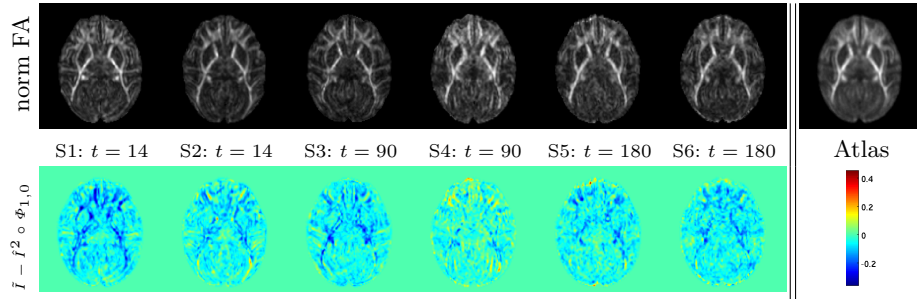


Fig. 6. Subject warping results to demonstrate the alignment of subjects at different time-points to an atlas at $t = 97$ as computed by the transformation composition of Eq. 8. [Top] Central axial slices of six arbitrarily selected measured subject time-points warped to atlas space show the final alignment quality (S# indicates subject number). [Top:Right] The central axial slice from the computed atlas time-point at $t = 97$. [Bottom] Absolute differences between the histogram matched FA images warped to atlas space and the computed atlas show the residual image mismatches.

will be publicly disseminated on NITRC. Further, joint statistical modeling and atlas-building will be investigated.

The software is available in open-source form hosted on NITRC: Fluid Registration and Atlas Toolkit (FRAT) (<http://www.nitrc.org/projects/frat/>). The toolkit contains source code for executables and libraries that implement all component algorithms as well as the full longitudinal atlas construction pipeline.

Acknowledgements This material is based upon work supported by the National Science Foundation (NSF) under Grant Nos. (EECS-0925875, BCS-08-26844) and by the National Institutes of Health (NIH) under Grant Nos. (UL1-RR025747-01, MH086633, P01CA142538-01, AG033387, P30 HD03110, P50 MH078105-01A2S, and U54 EB005149). Any opinions, findings, and conclusions or recommendations expressed in this material are those of the author(s) and do not necessarily reflect the views of NSF or NIH.

References

1. D. Alexander, C. Pierpaoli, P. Basser, and J. Gee. Spatial transformations of diffusion tensor magnetic resonance images. *IEEE Transactions on Medical Imaging*, 20(11):1131–1139, 2001.
2. D. C. Alexander and J. C. Gee. Elastic matching of diffusion tensor images. *Comput. Vis. Image Underst.*, 77(9):233–250, 2000.
3. V. Arsigny, P. Fillard, X. Pennec, and N. Ayache. Log-Euclidean metrics for fast and simple calculus on diffusion tensors. *Magnetic Resonance in Medicine*, 56(2):411–421, 2006.
4. M. Beg, M. Miller, A. Trounev, and L. Younes. Computing large deformation metric mappings via geodesic flows of diffeomorphisms. *IJCV*, 61(2):139–157, 2005.

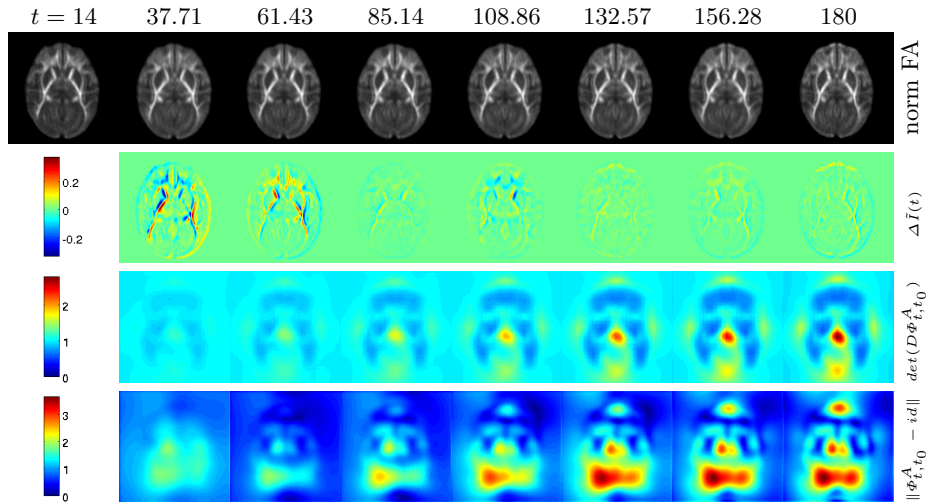


Fig. 7. Longitudinal atlas geometric growth. [Top] Central axial slices from the final longitudinal growth model show the geometric development of the population average from time 2 weeks through 6 months. The atlas is computed first by creating cross-sectional atlases from individual subject growth models, such as Fig. 5, at times 14, 55.5, 97, 138.5, and 180 days and then computing a growth model from these individual atlas time-points. The construction of the final growth model results in geometric correspondences for the atlas space across the entire time span. [Middle, top] Difference images computed between each time-point show the change between successive images (top row). These results show how the change tends to slow with increased age. [Middle, bottom] The determinant of the Jacobian of the coordinate map between 14 days and each intermediate time-point illustrates the local expansion and contraction. Since backwards maps are used, values larger than 1 indicate local contraction while values smaller than 1 indicate local expansion. When compared to the determinant of the Jacobian in Fig. 5, the result for the computed atlas shows a significantly more regular growth as is expected for a population average. [Bottom] The magnitude of displacement with respect to the initial time-point shows deformations (in mm) and indicates relatively symmetric deformations in atlas-space with most deformation occurring within the first 100 days of development.

5. B. Davis, P. Fletcher, E. Bullitt, and S. Joshi. Population shape regression from random design data. *Computer Vision, 2007. ICCV 2007. IEEE 11th International Conference on*, pages 1–7, 2007.
6. S. Durrleman, X. Pennec, G. Gerig, A. Trouvé, and N. Ayache. Spatiotemporal Atlas Estimation for Developmental Delay Detection in Longitudinal Datasets. Research Report RR-6952, INRIA, 2009.
7. A. C. Evans and the B.D.C. Group. The NIH MRI study of normal brain development. *NeuroImage*, 30:184–202, 2006.
8. S. Joshi, B. Davis, M. Jomier, and G. Gerig. Unbiased diffeomorphic atlas construction for computational anatomy. *NeuroImage*, 23(Supplement 1):S151 – S160, 2004. Mathematics in Brain Imaging.

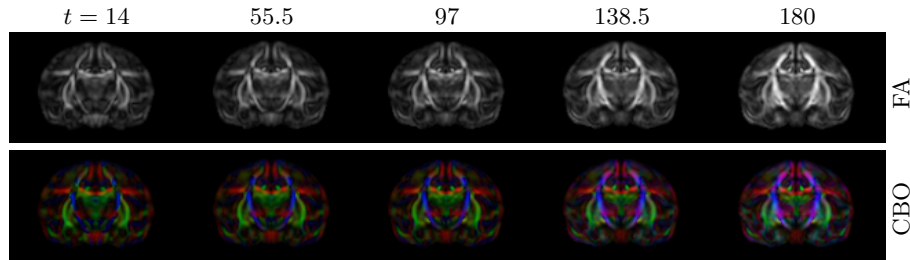


Fig. 8. Tensor atlas. Displacement maps were calculated from every measured input image to the geometric space of time-point 97 and all tensors were realigned into this space. From these tensors, an average tensor at a series of time points were calculated using the statistical modeling described in Section 3.3. These average tensor images were then geometrically aligned to the computed atlas at the corresponding time-points using the final atlas-space time series. [Top] FA images (not histogram normalized) computed from the average tensors show the geometric change as well as the overall anisotropy increases with age. [Bottom] Color by orientation images over time show an increase in diffusivity (brighter colors) with age.

9. A. R. Khan and M. F. Beg. Representation of time-varying shapes in the large deformation diffeomorphic framework. In *Proceedings of the International Symposium on Biomedical Imaging (ISBI)*, pages 1521–1524, 2008.
10. K. Liang and S. Zeger. Longitudinal data analysis using generalized linear models. *Biometrika*, 73(1):13, 1986.
11. M. Miller. Computational anatomy: shape, growth, and atrophy comparison via diffeomorphisms. *Neuroimage*, 23:S19–S33, 2004.
12. P. Mukherjee and R. C. McKinstry. Diffusion tensor imaging and tractography of human brain development. *Neuroimaging Clinics of North America*, 16(1):19 – 43, 2006. Advanced Pediatric Imaging.
13. M. Niethammer, G. Hart, and C. Zach. An optimal control approach for the registration of image time series. In *Proceedings of the Conference on Decision and Control*, pages 2427–2434, 2009.
14. P. Rakic and P. S. Goldman-Rakic. The development and modifiability of the cerebral cortex. overview. *Neuroscience Research Progress Bulletin*, 20(4):433–438, 1982.
15. J. Ruiz-Alzola, C.-F. Westin, S. K. Warfield, C. Alberola, S. E. Maier, and R. Kikinis. Nonrigid registration of 3d tensor medical data. *Medical Image Analysis*, 6(2):143–161, 2002.
16. D. Shen and C. Davatzikos. Measuring temporal morphological changes robustly in brain MR images via 4-dimensional template warping. *NeuroImage*, 21:1508–1517, 2004.
17. A. Trounev and L. Younes. Metamorphoses Through Lie Group Action. *Foundations of Computational Mathematics*, 5(2):173–198, 2005.
18. B. Yeo, T. Vercauteren, P. Fillard, J.-M. Peyrat, X. Pennec, P. Golland, N. Ayache, and O. Clatz. DT-REFinD: Diffusion Tensor Registration With Exact Finite-Strain Differential. *IEEE Transactions on Medical Imaging*, 28(12):1914–1928, 2009.
19. U. Yoon, V. S. Fonov, D. Perusse, A. C. Evans, and B. D. C. Group. The effect of template choice on morphometric analysis of pediatric brain data. *NeuroImage*, 45(3):769–777, 2009.